Acta Oceanol. Sin., 2022, Vol. 41, No. 12, P. 18–26
https://doi.org/10.1007/s13131-022-2066-5
http://www.aosocean.com
E-mail: ocean2@hyxb.org.cn

Sea level rise along China coast in the last 60 years

Hui Wang[1], Wenshan Li[1], Wenxi Xiang[1]*

[1] National Marine Data and Information Service, Tianjin 300171, China

Received 20 April 2022; accepted 1 May 2022

Abstract

Based on long-term tide gauge observations in the last 60 years, the temporal and spatial variation characteristics of sea level change along the coast of China are analyzed. The results indicate that the sea level along the coast of China has been rising at an increasing rate, with an estimated acceleration of 0.07 mm/a^2. The rise rates were 2.4 mm/a, 3.4 mm/a and 3.9 mm/a during 1960–2020, 1980–2020 and 1993–2020, respectively. In the last 40 years, the coastal sea level has risen fastest in the South China Sea and slowest in the Yellow Sea. Seasonal sea levels all show an upward trend but rise faster in winter and spring and slower in autumn. Sea level change along the coast of China has significant periodic oscillations of quasi-2 a, 4 a, 7 a, 11 a, quasi-19 a and 30–50 a, among which the 2–3 a, 11 a, and 30–50 a signals are most remarkable, and the amplitude is approximately 1–2 cm. The coastal sea level in the most recent decade reached its highest value in the last 60 years. The decadal sea level from 2010 to 2019 was approximately 133 mm higher than the average of 1960–1969. Empirical orthogonal function analysis indicates that China's coastal sea level has been changing in a north-south anti-phase pattern, with Pingtan and Fujian as the demarcation areas. This difference was especially obvious during 1980–1983, 1995–1997 and 2011–2013. The coastal sea level was the highest in 2016, and this extreme sea level event was analyzed to be related mainly to the anomalous wind field and ENSO.

Key words: sea level, long-term change, tide gauge records, spatial and temporal variability

Citation: Wang Hui, Li Wenshan, Xiang Wenxi. 2022. Sea level rise along China coast in the last 60 years. Acta Oceanologica Sinica, 41(12): 18–26, doi: 10.1007/s13131-022-2066-5

1 Introduction

Affected by anthropogenic activities and natural factors, the world is experiencing changes characterized by warming over the past 100 years (WMO, 2019; Cook et al., 2016; IPCC, 2014). Ocean warming and thermal expansion, mass loss from ice sheets and glaciers, and terrestrial water storage fluxes have led to continuous global sea level rise (IPCC, 2014, 2019). Proxy and instrumental sea level data indicate a transition in the late 19th century to the early 20th century from a relatively slow rise over the previous two millennia to a faster rise rate. The rise rate of the global mean sea level (GMSL) was 1.7 mm/a during 1901–2010, 2.0 mm/a during 1971–2010, and 3.2 mm/a during 1993–2010 (IPCC, 2014). From 1993 to 2019, the rise rate of the GMSL was (3.24±0.3) mm/a. In 2019, the GMSL continued to rise, reaching its highest since the beginning of the high-precision altimetry record (WMO, 2020).

In step with the GMSL, China's coastal sea level has continued to be high in recent years. During 1993–2019, the sea level rise rate along the coast of China was 3.9 mm/a, higher than the global mean (MNR, 2020; WMO, 2020). Moreover, the frequency of seasonal to annual sea level anomalies and the extreme sea level have all increased significantly. Sea level rise along the coast of China is mainly contributed by global sea level rise, regional hydrogeological and meteorological changes (Cai, 2010; Gao et al., 2016; Gregory et al., 2001; Ablain et al., 2017; Willis et al., 2008), and vertical land movement in coastal areas (Liu et al., 2015). Many previous studies have focused on determining global mean geocentric rates of change (also referred to as "absolute" changes), and to date, most coastal risk assessments have been undertaken using global-average projections of geocentric sea level rise (SLR). However, from a coastal management and planning perspective, regional or local relative sea level changes (i.e., changes relative to the level of the land) are important (Wahl et al., 2013; Nicholls et al., 2011; Nicholls and Cazenave, 2010). Additionally, the occurrence of ENSO will affect the activities of the East Asian monsoon through processes such as atmospheric teleconnection (Cai and Su, 2018), thus affecting sea level changes along the coast of China. China has a continental coastline of over 18 000 km with a dense economy and population (Zhang and Ouyang, 2019) as well as spatially diverse marine climate change features (Fan and Li, 2006). The accelerated rise in coastal sea level and extreme sea level events may have major impacts on the social and natural ecological environment in Chinese coastal areas, resulting in tidal flat loss, lowland inundation and ecological environment damage, as well as disasters such as storm surges and floods in coastal cities (Gregory et al., 2001; Hamilton, 2005; Fan and Li, 2006; McGranahan et al., 2007; Cai et al., 2009; Arnell and Lloyd-Hughes, 2014; Le Cozannet et al., 2014; Gao et al., 2014; Zhao et al., 2014; Fang et al., 2017; Liu et al., 2019; Li et al., 2019). Coastal communities are increasingly aware of the threats and serious challenges of sea level rise and the importance and urgency of taking common measures to reduce and prevent climate risks (Addo, 2013; Barbier, 2015; Cui et al., 2015; Hereher, 2015; Gutiérrez et al., 2016).

In recent years, several studies have been conducted focusing on coastal sea level changes in the China seas (Qu et al., 2019; Chen et al., 2018; Cheng et al., 2016). However, due to the limited tide gauge data and the discontinuous, limited up-to-date and

*Corresponding author, E-mail: xwx@nmdis.org.cn

possible uniformity of datasets, the spatial and temporal characteristics of sea level change along the coast of China may not be fully described. In this paper, long-term tide observation data from the China Ocean Observatory Network were used to comprehensively analyze the long-term trend, significant period and regional variation characteristics of coastal sea level change, as well as the extreme sea level events along the coast of China over the last 60 years. To eliminate in-homogenization of sea level data, multiple intensive quality controls were conducted, including datum plane unification, short-term missing data interpolation, and long-term sequence uniformity correction.

2 Materials and methodology

2.1 *Sea level data*

The sea level data come from the National Ocean Observatory Network of China. A total of 42 tide gauges with uniform station distribution, long observation time, good representativeness and continuous data were selected and recorded from January 1960 to December 2019. Multiple quality controls were conducted, including datum plane unification, short-term missing data interpolation, and long-term sequence uniformity correction (Wang et al., 2013). The details of the stations used are shown in Tables 1 and 2. Here, we attempt to improve the understanding of coastal relative sea level rise using a sufficiently uniform and spatially intensive dataset. The year 1993–2011 was defined as the baseline period, considering the 19 a oscillation period of sea level.

Table 1. Full names of the tide gauge stations

Name	Abbr.	Name	Abbr.	Name	Abbr.
Bayuquan	BYQ	Rizhao	RZH	Dongshan	DSN
Huludao	HLD	Lianyungang	LYG	Yunwo	YWO
Zhimaowan	ZMW	Lvsi	LSI	Shanwei	SWI
Qinhuangdao	QHD	Dajishan	DJS	Chiwan	CWN
Tanggu	TGU	Tanxu	TXU	Dawanshan	DWS
Longkou	LKO	Shengshan	SSH	Zhapo	ZPO
Xiaochangshan	XCS	Changtu	CTU	Naozhou	NZU
Laohutan	LHT	Zhenhai	ZHI	Beihai	BHI
Yantai	YTI	Shipu	SPU	Fangchenggang	FCN
Penglai	PLI	Dachen	DCN	Weizhou	WZU
Chengshantou	CST	Kanmen	KMN	Haikou	HKO
Qianliyan	QLY	Sansha	SSA	Qinlan	QLN
Xiaomaidao	XMD	Pingtan	PTN	Sanya	SYA
Wumatou	WMT	Xiamen	XMN	Dongfang	DFG

Table 2. Availability and time length of tide gauge stations used in the present study

Station	Duration	Station	Duration	Station	Duration
BYQ	1980–2020	RZH	1968–2020	DSN	1960–2020
HLD	1961–2020	LYG	1960–2020	YWO	1993–2020
ZMW	1983–2020	LSI	1976–2020	SWI	1971–2020
QHD	1965–2020	DJS	1978–2020	CWN	1986–2020
TGU	1960–2020	TXU	1978–2020	DWS	1984–2020
LKO	1963–2020	SSH	2000–2020	ZPO	1960–2020
XCS	1980–2020	CTU	1960–2020	NZU	1960–2020
LHT	1980–2020	ZHI	1966–2020	BHI	1967–2020
YTI	1960–2020	SPU	2000–2020	FCN	2000–2020
PLI	2000–2020	DCN	1980–2020	WZU	1964–2020
CST	1981–2020	KMN	1960–2020	HKO	1976–2020
QLY	1990–2020	SSA	1964–2020	QLN	1977–2020
XMD	1990–2020	PTN	1967–2020	SYA	2000–2020
WMT	2000–2020	XMN	1960–2020	DFG	1965–2020

2.2 *Methods*

2.2.1 *Statistical methods*

Harmonic analysis was used to estimate the linear trend of sea level change. The equation used for the computation is as follows:

$$H(t) = a + bt + \sum_{j=1}^{L} h_j \cos(\sigma_j t - \theta_j), \tag{1}$$

where a is the multiyear average sea level, b represents the rate of sea level change, L is the number of long-period signals, h_j, σ_j and θ_j are the amplitude, angular velocity, and phase of the jth major long-period signal, respectively.

Empirical orthogonal function decomposition analysis (EOF) (Hannachi et al., 2007; Wilks, 2011) was used across the stations along the coast of China to determine the dominant patterns of sea level change. First, the sea level data in the temporal and spatial fields were processed for anomalies, which are given in the form of the following matrix,

$$\boldsymbol{X} = \begin{bmatrix} x_{11} & x_{12} & \cdots & x_{1j} & \cdots & x_{1n} \\ x_{21} & x_{22} & \cdots & x_{2j} & \cdots & x_{2n} \\ \vdots & \vdots & \vdots & \vdots & \vdots & \vdots \\ x_{i1} & x_{i2} & \cdots & x_{ij} & \cdots & x_{in} \\ \vdots & \vdots & \vdots & \vdots & \vdots & \vdots \\ x_{m1} & x_{m2} & \cdots & x_{mj} & \cdots & x_{mn} \end{bmatrix}, \tag{2}$$

where m and n are the number of observations and stations, respectively (m>n). Each element is decomposed into the sum of the orthogonal time function and the orthogonal spatial function, which can be expressed as follows:

$$\hat{x} = \sum_{i,j} t_{hi} l_{hj}, \qquad \begin{matrix} i = 1, 2, \cdots, m \\ j = 1, 2, \cdots, n \end{matrix}, \tag{3}$$

where l_{hj} represents the spatial coefficient of the typical field h at the jth point, which is spatially dependent. t_{hi} represents the time coefficient of the typical field h at the ith observation time, which is temporally dependent. The above function can also be expressed as follows:

$$\boldsymbol{X}_{m\times n} = \boldsymbol{T}_{m\times m} \boldsymbol{L}_{m\times n}, \tag{4}$$

where

$$\boldsymbol{T}_{m\times m} = \begin{pmatrix} t_{11} & \cdots & t_{1m} \\ \vdots & & \vdots \\ t_{m1} & \cdots & t_{mm} \end{pmatrix}, \boldsymbol{L}_{m\times n} = \begin{pmatrix} l_{11} & \cdots & l_{1n} \\ \vdots & & \vdots \\ l_{m1} & \cdots & l_{mn} \end{pmatrix}. \tag{5}$$

The wavelet transform (Farge, 1992; Lau and Weng, 1995) was used to analyze mean sea level changes in both the time and the frequency domains. The wavelet transform of time function is defined as follows:

$$W(\tau, s) = \frac{1}{\sqrt{s}} \int_{-\infty}^{+\infty} f(t)\psi^* \times [(t-\tau)/s]\mathrm{d}t, \tag{6}$$

where τ is the localized time index, s is the wavelet scale, ψ is the wavelet mother function and the * denotes the complex conjugate. Here, the Morlet wavelet was chosen as the mother function and is formulated as follows:

$$\psi(\eta) = \pi^{-1/4} e^{i\omega_0 \eta} e^{-\eta^2/2}, \tag{7}$$

where η is the nondimensional time parameter. ω_0 is the nondimensional frequency, which has a value of 6 to satisfy the admissibility condition (Farge, 1992). The discrete Fourier transform algorithm was used in the calculation of Eqs (5) and (6) (Torrence and Compo, 1998).

The wavelet mother function $\psi(\eta)$ is complex and can be decomposed into real and imaginary parts, the results in the time-frequency domain can be presented in three ways: the real part, the modulus, or the phase of $W(\tau, s)$. We chose to represent on a time-frequency map the real part in the following discussion.

The wavelet power spectrum as $|W|^2$ can be defined. For the global wavelet spectrum, let us consider a vertical slice through a wavelet plot as a measure of the local spectrum. The time-averaged wavelet spectrum over all certain periods or all the local wavelet spectra is then expressed as follows:

$$\overline{W}^2(s) = \frac{1}{T}\sum_{\tau=0}^{T-1} |W_\tau(s)|^2, \tag{8}$$

where T is the number of points in a time series. The time-averaged wavelet spectrum is called the global wavelet spectrum (Torrence and Compo, 1998).

2.2.2 *Estuarine coastal ocean model*

To further attribute the extreme sea level events, a numerical model of the northwest Pacific was established based on the estuarine coastal ocean model (ECOM) v1.3 (Blumber and Mellor, 2013). The horizontal resolution of the model calculation was 5′×5′, and the range of domain was 15°–45°N, 105°–135°E. The bathymetry was interpolated based on the ETOPO5 dataset, and 10 Sigma layers were divided vertically. The upper boundary of meteorology applied the analysis wind datasets of ERA-Interim (Dee et al., 2011). A zero initial condition was adopted to produce the hourly sea level and offshore current, thus the monthly mean sea level and current were calculated based on the hourly result, reflecting the status of wind-driven current as well as sea surface height anomaly.

3 Results and discussion

3.1 *Long-term sea level change*

3.1.1 *Annual-mean sea level*

Coastal SLR was analyzed without correcting for vertical land motion since relative sea level is more essential when assessing coastal flood risk. Since the 1960s, the SLR along the coast of China has generally fluctuated and experienced three significant uplifts, showing an accelerated upward trend, and the estimated acceleration is 0.07 mm/a^2. The rise rate was 2.4 mm/a from 1960 to 2020 and 3.4 mm/a during 1980–2020. Particularly, from the satellite altimetry era of 1993 to 2020, the SLR rate along the coast of China was 3.9 mm/a, higher than the global mean (3.3 mm/a). The SLR along the coast of China remained high during 2012–2020 and over the last 60 years, with the highest level in 2016, followed by that in 2012 (Fig. 1).

The SLR rates at 42 representative stations since records began indicated regional differences along the coast of China, attributed to ENSO, wind, and local hydrodynamic processes (Wang et al., 2017). At the local scale, the observed interannual sea level variability was strongest at locations along the coasts of the Liaodong Peninsula, Laizhou Bay, Hangzhou Bay and Hainan Island, where the SLR rates ranged 3–4 mm/a. The rise rates were relatively low in western Liaodong Bay, Fujian and Guangxi, with values of approximately 1–2.5 mm/a (Table 3).

There is a spatially difference pattern in the SLR rate along the coast of China. From 1980 to 2020, the coastal sea level rise rates of the Bohai Sea, the Yellow Sea, the East China Sea and the South China Sea were 3.4 mm/a, 3.1 mm/a, 3.4 mm/a and 3.6 mm/a, respectively, which were the fastest in the South China Sea, followed by that in the Bohai Sea and the East China Sea, and they were the slowest in the Yellow Sea. From 2008 to 2012, the sea level along the Bohai Sea rose by 60 mm, with an annual rise rate as high as 15 mm/a, and the sea level was the highest in 2014. The sea level along the Yellow Sea coast was at its highest during 2012–2016 in the last 40 years but dropped significantly by 45 mm in 2017. In the East China Sea, the coastal sea level rose abnormally by 65 mm from 2011 to 2012 and reached its highest level in 2016. In the South China Sea, the coastal sea level rose by 68 mm from 2015 to 2017 and reached its highest level in 2017 (Fig. 2).

Several representative tide gauge stations were chosen to indicate significant increases with interannual and interdecadal periodic oscillations in the last 40 years in the China coastal waters. There were significant regional correlations in the sea level change series. The coastal sea level from Guangdong to Hainan, south Shandong to north Fujian, Bohai Sea and Laizhou Bay and the northern part of the Yellow Sea all increased significantly, with an average increase exceeding 100 mm. Among these stations, LKO, LSI, TXU, HKO and DFG all increased by more than 150 mm. The coastal SLR in the YTI and BHI was relatively small, at less than 50 mm (Fig. 3).

3.1.2 *Seasonal mean sea level*

The seasonal mean sea level along the coast of China showed an upward trend over the last 60 years. The rise rate was 2.4 mm/a for winter (December to February), 2.3 mm/a for spring (March to May), 2.0 mm/a for summer (June to August), and 2.3 mm/a for autumn (September to November) from 1960 to 2020. Except

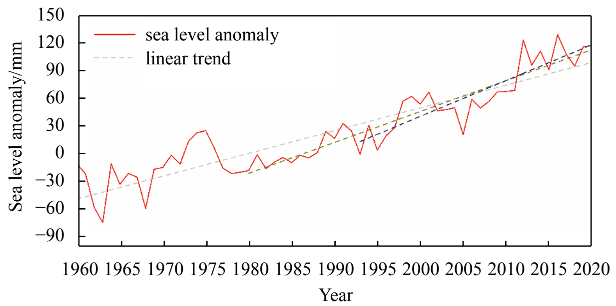

Fig. 1. The mean sea level showed a step-by-step accelerated upward trend along the coast of China since the tide gauge record began. The dotted lines indicate linear trends with higher rates of sea level rise from the three latest periods. Most of the tide gauges along the coast of China were established after 1960, and tide gauge observations have significantly improved since 1980.

Table 3. Sea level rise rate of representative stations along the coast of China since records began

Station	Rate/(mm·a^{-1})	Period	Station	Rate/(mm·a^{-1})	Period	Station	Rate/(mm·a^{-1})	Period
BYQ	3.7	1980–2020	RZH	2.2	1968–2020	DSN	1.7	1960–2020
HLD	1.9	1961–2020	LYG	0.9	1960–2020	YWO	2.9	1993–2020
ZMW	0.7	1983–2020	LSI	4.6	1976–2020	SWI	2.6	1971–2020
QHD	1.1	1965–2020	DJS	3.3	1978–2020	CWN	3.9	1986–2020
TGU	3.9	1960–2020	TXU	4.6	1978–2020	DWS	4.8	1984–2020
LKO	3.2	1963–2020	SSH	2.7	2000–2020	ZPO	2.5	1960–2020
XCS	2.7	1980–2020	CTU	3.2	1960–2020	NZU	2.3	1960–2020
LHT	3.7	1980–2020	ZHI	2.4	1966–2020	BHI	2.0	1967–2020
YTI	1.0	1960–2020	SPU	4.4	2000–2020	FCN	2.9	2000–2020
PLI	3.3	2000–2020	DCN	3.0	1980–2020	WZU	2.9	1964–2020
CST	2.6	1981–2020	KMN	2.5	1960–2020	HKO	4.6	1976–2020
QLY	2.5	1990–2020	SSA	2.0	1964–2020	QLN	4.2	1977–2020
XMD	2.2	1990–2020	PTN	2.5	1967–2020	SYA	6.1	2000–2020
WMT	0.4	2000–2020	XMN	2.0	1960–2020	DFG	3.1	1965–2020

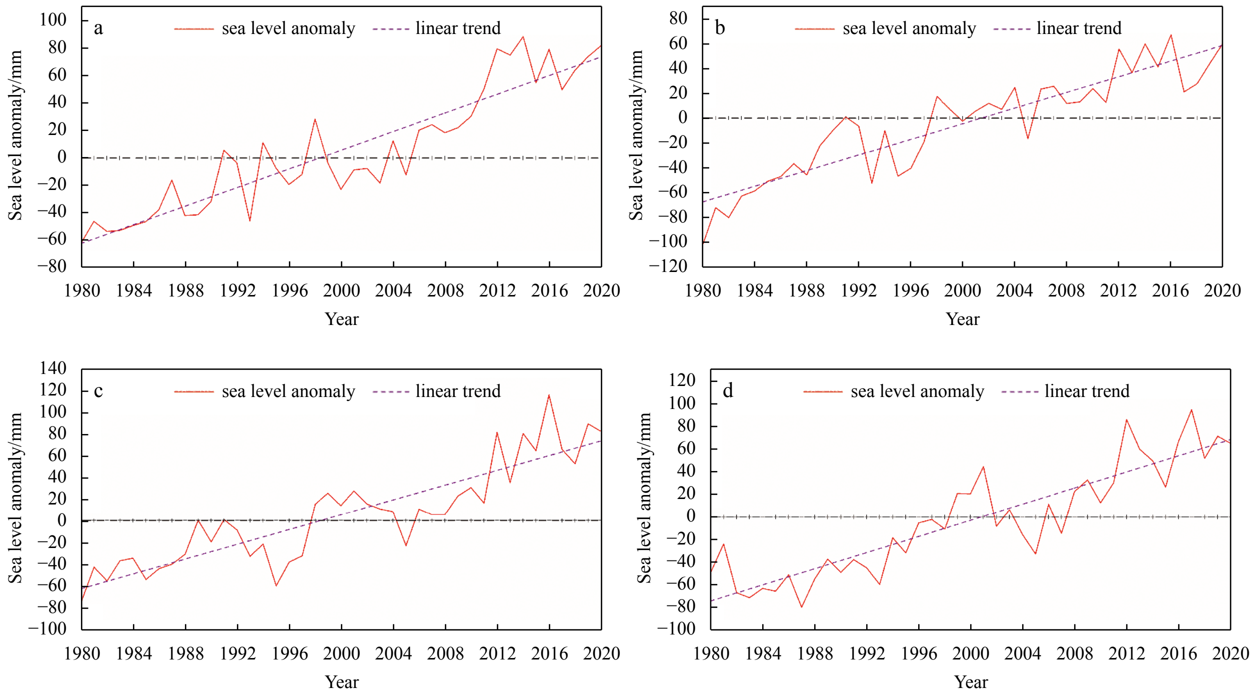

Fig. 2. Mean coastal sea level changes in the Bohai Sea (a), Yellow Sea (b), East China Sea (c) and South China Sea (d) from 1980 to 2020. The coastal sea level of sea areas has reached high levels in recent years, with the records being highest in 2014, 2016, 2016 and 2017.

for linear trends, the seasonal mean SLR has been accelerating, although it varies in different periods. The SLR rates were 3.7 mm/a, 3.0 mm/a, 2.9 m/a and 3.6 mm/a for winter, spring, summer and autumn, respectively, from 1980 to 2020. Furthermore, the seasonal mean sea level indicated a more significant rise since 1993, with higher rise rates of 3.6 mm/a, 3.4 mm/a, 3.6 mm/a and 4.5 mm/a for winter, spring, summer and autumn, respectively. The rate of SLR was the highest in winter for both periods of 1960–2020 and 1980–2020, while it was the highest in autumn during 1993–2020. Corresponding with the anomalous annual highs in 2012 and 2016, the coastal sea levels from summer to autumn in 2012 and in spring and autumn of 2016 all reached the historical highest values (Fig. 4).

3.2 *Interannual and decadal sea level change*

To analyze the interannual and decadal sea level changes along the coast of China, a linear trend was first removed from the annual mean sea level series. Morlet wavelet transform analysis was performed on the residual sea level anomalies with a time length of approximately 60 years. The results showed that the wavelet real coefficient formed the center of oscillation between the positive and negative phases of various time scales, indicating that the coastal sea level contained significant multiscale periodic changes. Combining the amplitudes on the right side, the significant periods of coastal sea level change mainly included quasi-2 a, 4 a, 7 a, 11 a, quasi 19 a and 30–50 a in the 95% confidence interval. The oscillation period of 2–3 a was from coastal hydrological and meteorological elements. It is common that short-term coastal sea level changes are closely related to local wind, flow and sea surface temperature. Another component was the 4–7 a cycle, which is believed to be closely related to the ENSO phenomenon. The correlation between the sea

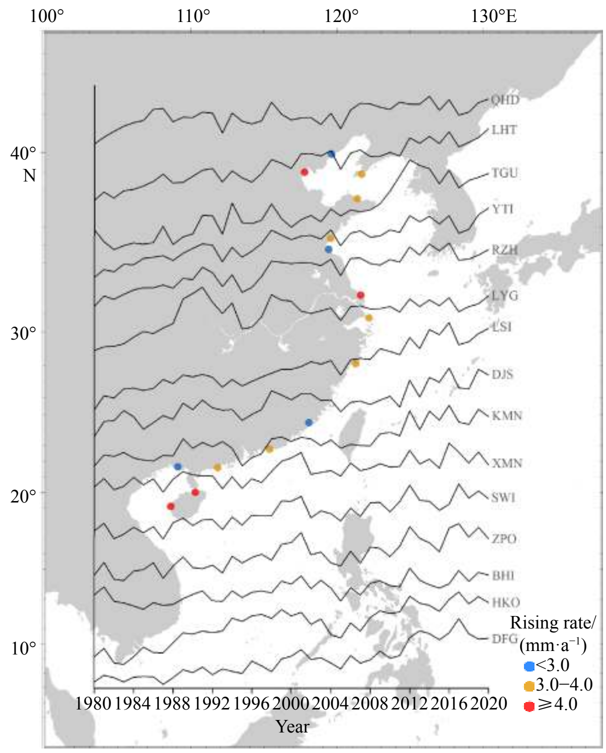

Fig. 3. Mean sea level changes at representative stations along the coast of China from 1980 to 2020 show significant regional correlations, and coastal sea level rise rates are higher at TGU, LSI, HKO and DFG.

level of the Chinese seas and the sea temperature in the central and eastern equatorial areas was significant, and the coefficients increased from north to south along the coast of China, with values greater than that of 0.69 in the South China Sea (Wang et al., 2018b). The cycle of quasi 11 a reflects the influence of sunspots on sea level change. The 9 a and 19 a cycles are astronomical tide cycles, reflecting the changes in lunar declination, known as intersection tides. Additionally, it could be concluded from the results of wavelet transform analysis that the periodic oscillations of 2–3 a, 11 a, and 30–50 a have been most significant in the last 60 years, with amplitudes of approximately 1–2 cm (Wang et al., 2018a). These signals were followed by oscillations 4 a, 7 a and quasi 19 a, with amplitudes of approximately 0.5–1 cm (Fig. 5).

Decadal sea level change is also an important indicator of long-term climate change. The coastal sea level in the 1960s was the lowest in the last 60 years. After a slight rebound in the 1970s, it declined again in the 1980s and continued to rise afterwards. The sea level in the last decade was the highest. In particular, the mean sea level from 2010 to 2019 was 133 mm, 105 mm, and 72 mm higher than the average from 1960–1969, 1980–1989, and 1990–1999, respectively (Fig. 6).

The decadal sea level change along the coast of China presented significant regional and temporal differences. During 1980–1989, the coastal sea levels of the Yellow Sea and the South China Sea were generally low. During 1990–1999, the sea levels of the Yellow Sea, East China Sea and South China Sea were generally low, while the sea level of the Bohai Sea increased greatly. From 2000 to 2009, the sea levels in the Yellow Sea, the East China Sea and the South China Sea all rose to a large extent. The SLR from 2010 to 2019 was the largest along the coast of the Bohai Sea, followed by that of the East China Sea, and it was smallest in the Yellow Sea (Table 4).

3.3 *Spatial and temporal sea level characteristics*

To investigate the spatial and temporal sea level change characteristics, EOF analysis of the annual mean sea level anomaly series along the coast of China from 1980 to 2020 was also conducted. As a result, the first mode of EOF was able to explain 81% of the total mean sea level anomaly, reflecting a significant rising trend. The sea level anomaly was higher in areas of the southw-

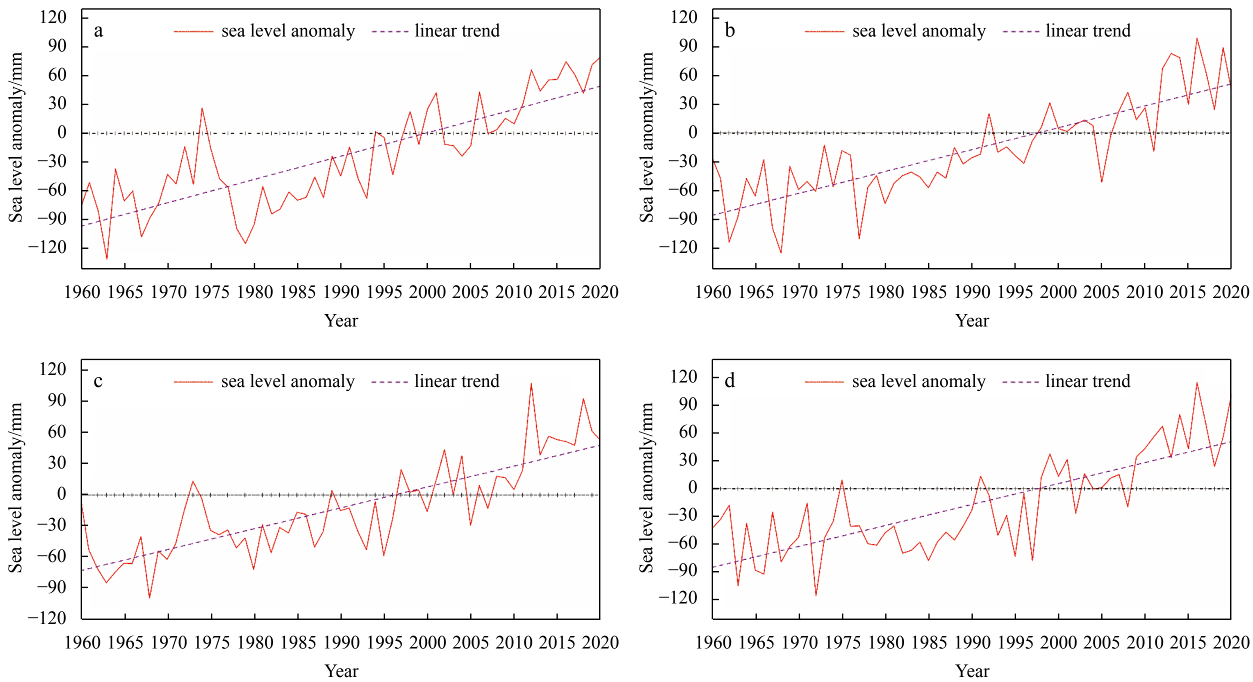

Fig. 4. The seasonal mean sea level along the coast of China rose acceleratively from 1960 to 2020 and was highest in winter. Winter (a); spring (b); summer (c); autumn (d).

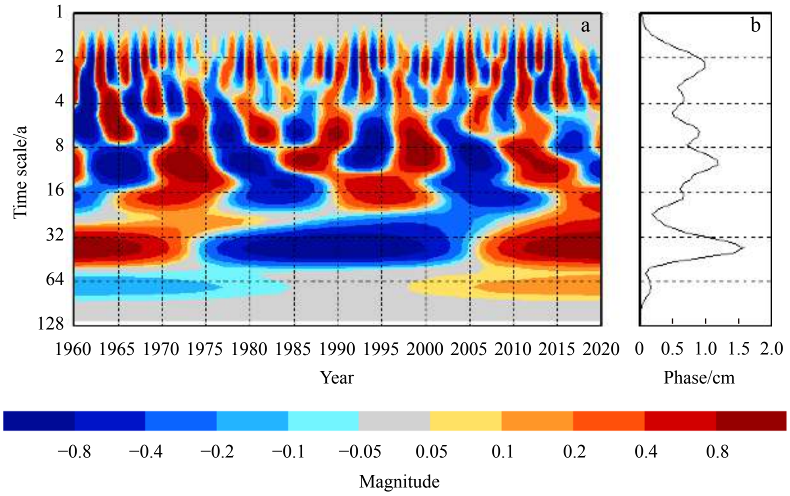

Fig. 5. The real part (a) and the amplitude (b) of the sea level wavelet transform along the coast of China indicated significant periodical changes from quasi-2 a to 30–50 a.

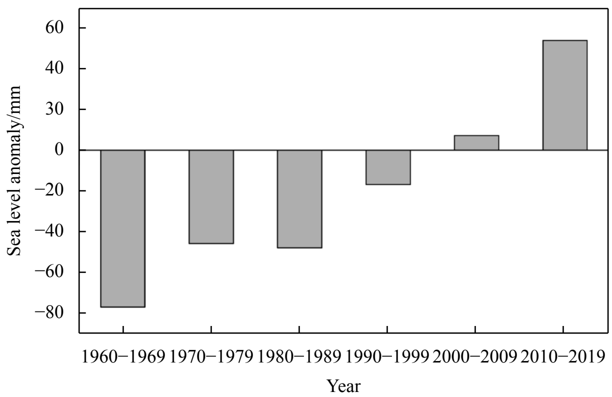

Fig. 6. Decadal mean sea levels along the coast of China have risen step-by-step since the 1960s.

Table 4. Decadal sea level anomaly of China seas from the 1960s (unit: mm)

Period	Bohai Sea	Yellow Sea	East China Sea	South China Sea
1980–1989	−45	−58	−42	−56
1990–1999	−8	−16	−17	−24
2000–2009	3	10	10	7
2010–2019	64	39	63	55

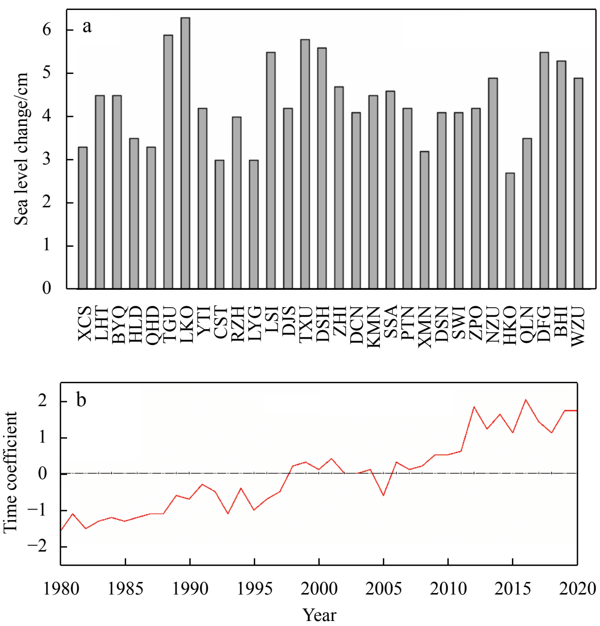

Fig. 7. The first mode empirical orthogonal function of sea level change (a) and the corresponding time coefficient (b) along the coast of China indicate an overall rise with spatial differences.

est Bohai Sea, south Jiangsu, Hangzhou Bay and Hainan coast, corresponding to rapid SLRs in these areas. The lower sea level anomaly indicated relatively slow SLR along the coast of west Liaodong Bay, north Jiangsu, west Taiwan Strait and the Beibu Gulf. From the aspect of the time coefficient, coastal SLR was generally slow in the 1980s. The coastal sea level was higher in the 1990s and rose significantly, especially in the late 1990s. The fluctuation of the time coefficient in approximately 2005 corresponded to the low sea level event in 2005 (Ministry of Natural Resources of the People's Republic of China, 2019). China's coastal sea level in the last decade has maintained a high historical level, which was also basically consistent with the characteristics of long-term sea level change shown in Fig. 7.

The second mode EOF was able to explain 6% of the total change. This modality mainly reflected the characteristics of the north-south anti-phase change in the China coastal sea level, divided by the coastal areas between Pingtan and Xiamen in Fujian Province. This is also in correspondence with the northward drop of coastal mean dynamic topography which undergoes an evident seasonality affected by counter balance of contributions from the alongshore wind and the coastal current (Lin et al., 2021). The annual mean sea level along the coast of China varied significantly from north to south before 2000. Especially from 1984 to 1994, the sea level anomalies along the coast of China were generally higher in the north than in the south. During the periods of 1980–1983, 1995–1997, 2011–2013 and 2017, the China coastal sea level anomalies showed significant north-low and south-high patterns (Fig. 8).

3.4 *Extreme sea level events along China coast*

Extreme sea levels can have devastating societal impacts

(Muis et al., 2016). Extreme sea level events along the coast of China have intensified under accelerating SLR (Feng et al., 2019; Wang et al., 2014). In 2016, the Chinese coastal sea levels reached their highest level since 1960, which was 82 mm higher than the multiyear average. The monthly sea levels in September, October, November and December all reached their highest historical values that were 104 mm, 113 mm, 126 mm and 109 mm higher than the multiyear average of the same period, respectively. In 2012, the Chinese coastal sea levels reached the second highest value since 1960, which was 76 mm higher than the multiyear average. The monthly sea levels in June, August and October all reached historical highs that were 114 mm, 130 mm and 97 mm higher than the multiyear average of the same period, respectively. The coincidence of several long-period oscillations (such as ENSO, sunspots, astronomical tide cycles), abnormal wind fields, tropical cyclones, ocean currents, and other factors all contributed to abnormally high sea levels. The extreme sea level event in 2016 occurred just after the 2015/2016 strong El Niño event and before the 2017/2018 La Niña event. The sea surface temperature changes in the central and eastern equatorial Pacific Ocean affect the activities of the East Asian monsoon through atmospheric teleconnection, thus affecting sea level changes along the coast of China (Fang et al., 2006; Han and Huang, 2009; Wang et al., 2018b). To quantitatively evaluate this influence, the wind-driven sea level anomaly was calculated by ECOM simulation. Cyclonic atmospheric circulation presented in the seas of China from September to November 2016, consisting of the southwest wind anomaly in the South China Sea, north wind anomaly in the East China Sea, and east wind anomaly in the Bohai Sea as well as in the Yellow Sea, which drove onshore seawater transportation in the north of the South China Sea (Fig. 9a). As a result, the height of wind-driven sea level in the Taiwan Strait and the north coast reached 40–90 mm, contributing 35%–80% to the sea level anomaly (Fig. 9b). At the same time, from September to October 2016, five cyclones impacted South China. The storm surge clusters caused 70–360 mm short-term high sea levels during influence periods.

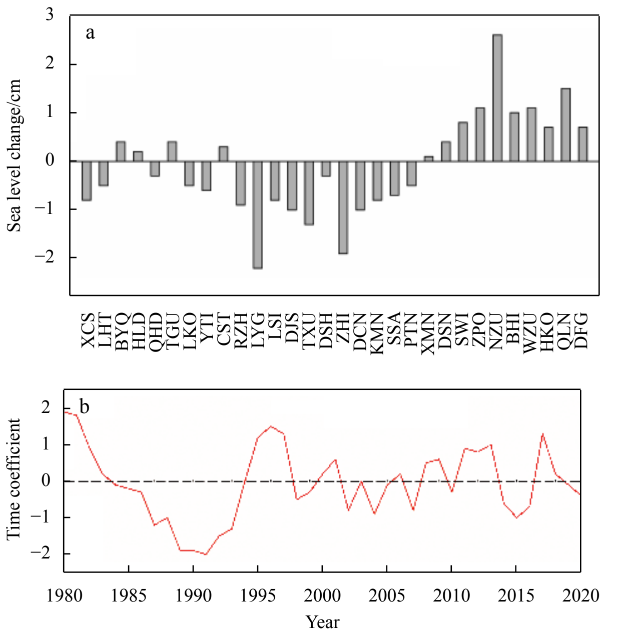

Fig. 8. The second mode empirical orthogonal function of sea level change (a) and the corresponding time coefficient (b) along the coast of China indicate the anti-phase spatial pattern in the last 40 years.

4 Conclusions

Tide data from long-term ocean observation stations along the coast of China were used to systematically analyze the temporal and spatial variation characteristics of China's coastal sea level over the last 60 years. The results indicated that China's coastal sea level rise has generally accelerated, and the estimated acceleration has been 0.07 mm/a^2. The coastal SLR rates in 1960–2020, 1980–2020 and 1993–2020 were 2.4 mm/a, 3.4 mm/a and 3.9 mm/a, respectively. In the last 40 years, the SLR rates at the Liaodong Peninsula, Laizhou Bay, Hangzhou Bay and Hainan Island were relatively high, ranging from 3–4 mm/a. The SLR

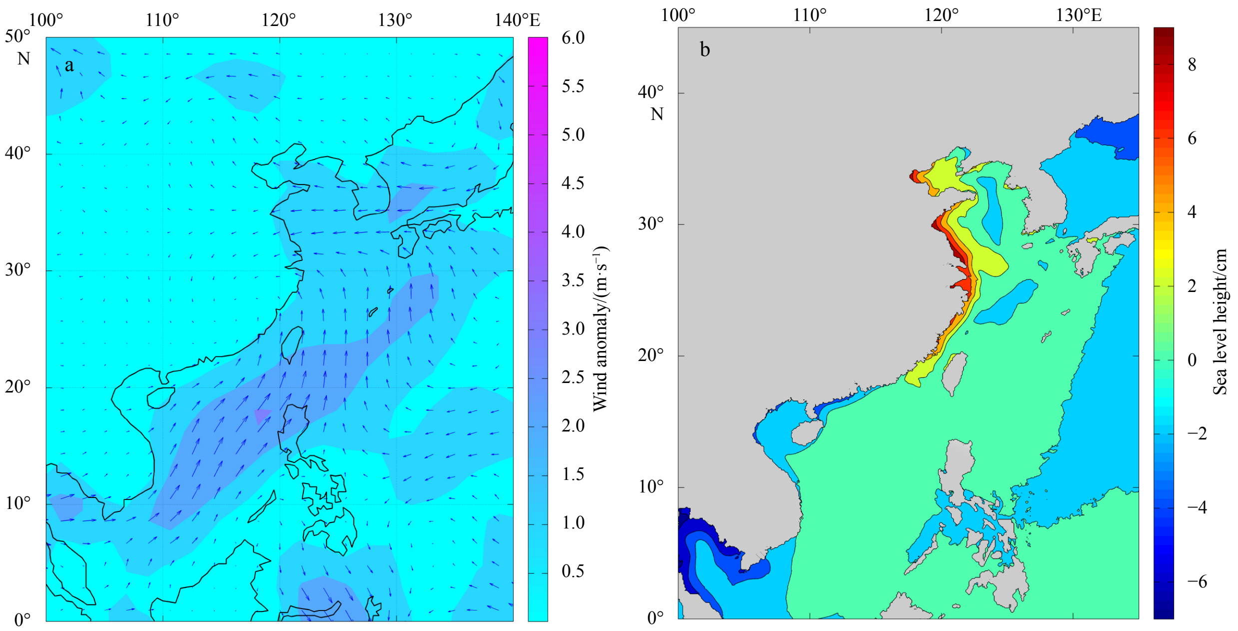

Fig. 9. Mean wind anomaly (a) and wind-driven sea level height (b) from September to November in the northwestern Pacific in 2016.

rates west of Liaodong Bay, Fujian and Guangxi were relatively low, ranging from 1–2.5 mm/a. On the scale of the China seas, coastal sea level rises fastest in the South China Sea and slowest in the Yellow Sea. In addition, there were significant differences in the seasonal SLR trends. From 1993 to 2020, China's coastal sea level rises fastest in autumn, with a rise rate of 4.5 mm/a. The SLR in summer and spring is slower, with a rise rate of 3.4 mm/a. Additionally, China's coastal sea level has been rising with significant cyclical oscillation. The main significant periods include quasi 2 a, 4 a, 7 a, 11 a, quasi 19 a and 30–50 a. For the decadal sea level change, the sea level in the 1960s was at its lowest value in nearly 60 years. After the 1980s, SLR accelerated and reached its highest level in the most recent decade. The mean sea level during 2010–2019 was 133 mm higher than the average during 1960–1969. Furthermore, coastal sea level change in the Chinese seas was characterized by a north-south anti-phase pattern, taking Pingtan as the demarcation area. Extreme sea level events were found to be related to anomalous wind, tropical cyclones and other factors; specifically, wind-driven sea level anomalies contributed to 40%–80% of the sea level anomaly from September to November 2016.

References

Ablain M, Legeais J F, Prandi P, et al. 2017. Satellite altimetry-based sea level at global and regional scales. Surveys in Geophysics, 38(1): 7–31, doi: 10.1007/s10712-016-9389-8

Addo K A. 2013. Assessing coastal vulnerability index to climate change: the case of Accra–Ghana. Journal of Coastal Research, 165(sp2): 1892–1897

Arnell N W, Lloyd-Hughes B. 2014. The global-scale impacts of climate change on water resources and flooding under new climate and socio-economic scenarios. Climatic Change, 122(1–2): 127–140

Barbier E B. 2015. Climate change impacts on rural poverty in low-elevation coastal zones. Estuarine, Coastal and Shelf Science, 165: A1–A13

Blumber A F, Mellor G L. 2013. A description of a three-dimensional coastal ocean circulation model. In: Heaps N S, ed. Three-Dimensional Coastal Ocean Models, Volume 4. Washington: American Geophysical Union, 1–16

Cai Rongshuo. 2010. Climate Change Influence on the Ecosystem in the China Offshore (in Chinese). Beijing: China Ocean Press

Cai Feng, Su Tonghua. 2018. Intraseasonal Variation of the East Asian Summer Monsoon Regulated by the ENSO Cycle. Beijing: China Meteorological Press

Cai Feng, Su Xianze, Liu Jianhui, et al. 2009. Coastal erosion in China under the condition of global climate change and measures for its prevention. Progress in Natural Science, 19(4): 415–426, doi: 10.1016/j.pnsc.2008.05.034

Chen Nan, Han Guoqi, Yang Jingsong. 2018. Mean relative sea level rise along the coasts of the China Seas from mid-20th to 21st centuries. Continental Shelf Research, 152: 27–34, doi: 10.1016/j.csr.2017.12.002

Cheng Yongcun, Ezer T, Hamlington B D. 2016. Sea level acceleration in the China Seas. Water, 8(7): 293, doi: 10.3390/w8070293

Cook J, Oreskes N, Doran P T, et al. 2016. Consensus on consensus: a synthesis of consensus estimates on human-caused global warming. Environmental Research Letters, 11(4): 048002, doi: 10.1088/1748-9326/11/4/048002

Cui Lifang, Ge Zhenming, Yuan Lin, et al. 2015. Vulnerability assessment of the coastal wetlands in the Yangtze Estuary, China to sea-level rise. Estuarine, Coastal and Shelf Science, 156: 42–51

Dee D P, Uppala S M, Simmons A J, et al. 2011. The ERA-Interim reanalysis: configuration and performance of the data assimilation system. Quarterly Journal of the Royal Meteorological Society, 137(656): 553–597, doi: 10.1002/qj.828

Fan Daidu, Li Congxian. 2006. Complexities of China's coast in response to climate change. Advances in Climate Change Research, 2(S1): 54–58

Fang Guohong, Chen Haiying, Wei Zexun, et al. 2006. Trends and interannual variability of the South China Sea surface winds, surface height, and surface temperature in the recent decade. Journal of Geophysical Research, 111(C11): C11S16, doi: 10.1029/2005JC003276

Fang Jiayi, Liu Wei, Yang Saini, et al. 2017. Spatial-temporal changes of coastal and marine disasters risks and impacts in Mainland China. Ocean & Coastal Management, 139: 125–140

Farge M. 1992. Wavelet transforms and their applications to turbulence. Annual Review of Fluid Mechanics, 24: 395–457, doi: 10.1146/annurev.fl.24.010192.002143

Feng Jianlong, Li Delei, Wang Tao, et al. 2019. Acceleration of the extreme sea level rise along the Chinese coast. Earth and Space Science, 6(10): 1942–1956, doi: 10.1029/2019EA000653

Gao Yi, Wang Hui, Liu Guimei, et al. 2014. Risk assessment of tropical storm surges for coastal regions of China. Journal of Geophysical Research, 119(9): 5364–5374, doi: 10.1002/2013JD021268

Gao Zhigang, Zhang Qinghe, Wang Hui, et al. 2016. The impacts of wind and air pressure on fluctuations of the mean Bohai Sea Level. Journal of Coastal Research, 74(sp1): 13–21

Gregory J M, Church J A, Boer G J, et al. 2001. Comparison of results from several AOGCMs for global and regional sea-level change 1900–2100. Climate Dynamics, 18(3–4): 225–240

Gutiérrez O, Panario D, Nagy G J, et al. 2016. Climate teleconnections and indicators of coastal systems response. Ocean & Coastal Management, 122: 64–76

Hamilton J M, Maddison D J, Tol R S J. 2005. Climate change and international tourism: a simulation study. Global Environmental Change, 15(3): 253–266, doi: 10.1016/j.gloenvcha.2004.12.009

Han Guoqi, Huang Weigen. 2009. Low-frequency sea-level variability in the South China Sea and its relationship to ENSO. Theoretical and Applied Climatology, 97(1): 41–52

Hannachi A, Jolliffe I T, Stephenson D B. 2007. Empirical orthogonal functions and related techniques in atmospheric science: a review. International Journal of Climatology, 27(9): 1119–1152, doi: 10.1002/joc.1499

Hereher M E. 2015. Assessment of South Sinai coastal vulnerability to climate change. Journal of Coastal Research, 31(6): 1469–1477

Intergovernmental Panel on Climate Change (IPCC). 2014. Summary for policymakers. In: IPCC, ed. Climate Change 2013: The Physical Science Basis. Working Group I Contribution to the Fifth Assessment Report of the Intergovernmental Panel on Climate Change. Cambridge: Cambridge University Press

Intergovernmental Panel on Climate Change (IPCC). 2019. Summary for policymakers. In: Pörtner H O, Roberts D C, Masson-Delmotte V, et al., eds. IPCC Special Report on the Ocean and Cryosphere in a Changing Climate. Cambridge: Cambridge University Press

Lau K M, Weng Hengyi. 1995. Climate signal detection using wavelet transform: how to make a time series sing. Bulletin of the American Meteorological Society, 76(12): 2391–2402, doi: 10.1175/1520-0477(1995)076<2391:CSDUWT>2.0.CO;2

Le Cozannet G, Garcin M, Yates M, et al. 2014. Approaches to evaluate the recent impacts of sea-level rise on shoreline changes. Earth-Science Reviews, 138: 47–60, doi: 10.1016/j.earscirev.2014.08.005

Li Wenshan, Wang Hui, Zhang Jianli, et al. 2019. Assessment on sandy coast erosion under sea level rise scenarios along Liaodong Bay. Marine Science Bulletin, 38(1): 31–37

Lin Wenqiang, Lin Hongyang, Hu Jianyu. 2021. The tilt of mean dynamic topography and its seasonality along the coast of the Chinese mainland. Journal of Geophysical Research, 126(2): e2020JC016778, doi: 10.1029/2020JC016778

Liu Shouhua, Chen Changlin, Liu Kexiu, et al. 2015. Vertical motions of tide gauge stations near the Bohai Sea and Yellow Sea. Science China Earth Sciences, 58(12): 2279–2288, doi: 10.1007/s11430-015-5167-6

Liu Bingjun, Peng Sihan, Liao Yeying, et al. 2019. The characteristics and causes of increasingly severe saltwater intrusion in Pearl

River Estuary. Estuarine, Coastal and Shelf Science, 220: 54–63, doi: 10.1016/j.ecss.2019.02.041

McGranahan G, Balk D, Anderson B. 2007. The rising tide: assessing the risks of climate change and human settlements in low elevation coastal zones. Environment and Urbanization, 19(1): 17–37, doi: 10.1177/0956247807076960

Ministry of Natural Resources of the People's Republic of China. 2019. China Sea Level Bulletin 2018 (in Chinese). Beijing: Ministry of Natural Resources of the People's Republic of China

Muis S, Verlaan M, Winsemius H C, et al. 2016. A global reanalysis of storm surges and extreme sea levels. Nature Communications, 7: 11969, doi: 10.1038/ncomms11969

Nicholls R J, Cazenave A. 2010. Sea-level rise and its impact on coastal zones. Science, 328(5985): 1517–1520, doi: 10.1126/science.1185782

Nicholls R J, Hanson S E, Lowe J A, et al. 2011. Constructing Sea-Level Scenarios for Impact and Adaptation Assessment of Coastal Area: A Guidance Document. Geneva: Supporting Material, Intergovernmental Panel on Climate Change Task Group on Data and Scenario Support for Impact and Climate Analysis (TGICA), 47

Qu Ying, Jevrejeva S, Jackson L P, et al. 2019. Coastal Sea level rise around the China Seas. Global and Planetary Change, 172: 454–463, doi: 10.1016/j.gloplacha.2018.11.005

Torrence C, Compo G P. 1998. A practical guide to wavelet analysis. Bulletin of the American Meteorological Society, 79(1): 61–78, doi: 10.1175/1520-0477(1998)079<0061:APGTWA>2.0.CO;2

Wahl T, Haigh I D, Woodworth P L, et al. 2013. Observed mean sea level changes around the North Sea coastline from 1800 to present. Earth-Science Reviews, 124: 51–67, doi: 10.1016/j.earscirev.2013.05.003

Wang Hui, Liu Kexiu, Fan Wenjing, et al. 2013. Data uniformity revision and variations of the sea level of the western Bohai Sea. Marine Science Bulletin, 32(3): 256–264

Wang Hui, Liu Kexiu, Fan Wenjing, et al. 2014. Analysis on the sea level anomaly high of 2012 in China coastal area. Haiyang Xuebao (in Chinese), 36(5): 8–17, doi: 10.3969/j.issn.0253-4193.2014.05.002

Wang Hui, Liu Kexiu, Fan Wenjing, et al. 2018a. Analysis on the sea level anomaly high of 2016 in China coastal area. Haiyang Xuebao (in Chinese), 40(2): 43–52

Wang Hui, Liu Kexiu, Gao Zhigang, et al. 2017. Characteristics and possible causes of the seasonal sea level anomaly along the South China Sea coast. Acta Oceanologica Sinica, 36(1): 9–16, doi: 10.1007/s13131-017-0988-0

Wang Hui, Liu Kexiu, Wang Aimei, et al. 2018b. Regional characteristics of the effects of the El Niño-Southern Oscillation on the sea level in the China Sea. Ocean Dynamics, 68(4–5): 485–495

Wilks D S. 2011. Statistical Methods in the Atmospheric Sciences. 3rd ed. Amsterdam: Academic Press, 704

Willis J K, Chambers D P, Nerem R S. 2008. Assessing the globally averaged sea level budget on seasonal to interannual timescales. Journal of Geophysical Research, 113(C6): C06015

World Meteorological Organization (WMO). 2019. WMO Statement on the State of the Global Climate in 2018. Geneva: WMO

World Meteorological Organization (WMO). 2020. WMO Statement on the State of the Global Climate in 2019. Geneva: WMO

Zhang Lu, Ouyang Zhiyun. 2019. Focusing on rapid urbanization areas can control the rapid loss of migratory water bird habitats in China. Global Ecology and Conservation, 20: e00801, doi: 10.1016/j.gecco.2019.e00801

Zhao Changjin, Ge Jianzhong, Ding Pingxing. 2014. Impact of sea level rise on storm surges around the Changjiang Estuary. Journal of Coastal Research, 68(sp1): 27–34